THE EFFECT OF TRUNCATION AND SHIFT ON VIRIAL COEFFICIENTS OF LENNARD–JONES POTENTIALS

Katherine R. S. SHAUL[1], Andrew J. SCHULTZ[2] and David A. KOFKE[3,*]

Department of Chemical and Biological Engineering, University at Buffalo, The State University of New York, Buffalo, NY 14260, USA; e-mail: [1] schadel2@buffalo.edu, [2] ajs42@buffalo.edu, [3] kofke@buffalo.edu

Received September 2, 2009
Accepted December 21, 2009
Published online April 15, 2010

Dedicated to Professor Ivo Nezbeda on the occasion of his 65th birthday.

We present virial coefficients of up to fifth order computed by Mayer-sampling Monte Carlo for several truncated-and-shifted Lennard–Jones potentials. We employ these coefficients within the virial equation of state to compute vapor-branch spinodals and critical points for each potential considered. We find that truncation distances of 5.0σ and higher yield values in significantly better agreement with those of the unmodified potential than those resulting from the more commonly used truncation distances of 2.5 and 3.0σ. We also employ these virial coefficients to examine the perturbed virial expansion method of Nezbeda and Smith for estimating the critical point. We find that the first-order perturbation performs well in characterizing the effect of potential truncation on the critical point for the truncation distances considered, with errors in critical temperatures ranging from –3 to +2% and errors in critical densities about constant at –22%. Addition of higher-order terms to the perturbation treatment brings it closer to the behavior given by the virial equation of state, which at fifth order underestimates the critical temperatures by 2 to 4% and the critical densities by 20 to 30%.

Keywords: Equation of state; Virial coefficients; Truncated-and-shifted Lennard–Jones potential; Mayer sampling; Monte Carlo method; Molecular modeling; Thermodynamics.

When employed in molecular simulations, the Lennard–Jones (LJ) potential, u^{LJ} (Eq. (*1*)), is often truncated to expedite calculations of fluid properties. The potential is then typically shifted up to avoid a discontinuity at the truncation distance. Common truncation distances are 2.5 and 3.0σ, as for these and larger truncation distances the truncated-and-shifted Lennard–Jones (LJTS) potential, u^{LJTS} (Eq. (*2*)), appears to be almost identical to the original.

Collect. Czech. Chem. Commun. 2010, Vol. 75, No. 4, pp. 447–462

doi:10.1135/cccc2009113

$$u^{\mathrm{LJ}}(r) = 4\varepsilon\left(\left(\frac{\sigma}{r}\right)^{12} - \left(\frac{\sigma}{r}\right)^{6}\right) \tag{1}$$

$$u^{\mathrm{LJTS}}(r) = \begin{cases} u^{\mathrm{LJ}}(r) - u^{\mathrm{LJ}}(r_{\mathrm{c}}) & r \le r_{\mathrm{c}} \\ 0 & r > r_{\mathrm{c}} \end{cases} \tag{2}$$

It is well known that these apparently minor modifications to the potential have a significant impact on fluid properties. For example, truncation at 2.5σ and shift results in a critical temperature about 17.8% lower than that of the unmodified potential[1]. This change can be mitigated through the application of correction terms after the simulation is completed, and in this manner the net effect of truncation and shift can be made of the same magnitude as other finite-size effects, as noted by Kolafa and Nezbeda[2].

Our understanding of how these minor modifications to the potential result in dramatic changes to the fluid properties is incomplete. As can be inferred from the pressure equation for pairwise additive, spherically symmetric potentials (Eq. (*3*)), truncation of the pair potential eliminates contributions to the pressure from attractive interactions beyond the cutoff, and it introduces an impulsive contribution at the cutoff, where the potential steps to zero[3]. The impulsive contribution would offset in part the repulsive effect of truncation on the pressure, but it is eliminated by the shift. The shift further affects the pressure by altering the radial distribution function, $g(r)$, within the truncation radius – thereby changing the number of interactions that contribute to the pressure.

$$P = \rho kT - \frac{\rho^2}{6}\int_0^{\infty} r\left(\frac{\partial u}{\partial r}\right) g(r) 4\pi r^2 \,\mathrm{d}r \tag{3}$$

To examine more closely how changes in the description of the interactions alter the pressure, we consider the virial equation of state (Eq. (*4*)). As cluster integrals over configuration space, the virial coefficients, B_n, provide a cumulative measure of how truncation and shift affect molecular interactions within groups of n molecules at different temperatures.

$$\frac{P}{\rho kT} = 1 + \sum_{n=2}^{\infty} B_n(T)\,\rho^{n-1} \tag{4}$$

The second virial coefficient, B_2 (Eq. (*5*)), is the simplest coefficient to calculate and to interpret with regard to truncation and shift. We observe that the change in the Lennard–Jones B_2 after truncation ($B_2^{\mathrm{LJT}} - B_2^{\mathrm{LJ}}$) and the change after shift ($B_2^{\mathrm{LJTS}} - B_2^{\mathrm{LJT}}$) are roughly equal (within 25% at $kT/\varepsilon = 0.7$ for truncation at 2.5σ) and both decrease and become more similar with increasing temperature and truncation distance. Higher-order B_n are generally much more sensitive to shift than truncation, as the high connectivity of the diagrams makes configurations with long separation distances between pairs relatively unimportant.

$$B_2 = -2\pi \int_0^\infty (\mathrm{e}^{-u/kT} - 1) r^2 \mathrm{d}r \tag{5}$$

Schultz and Kofke[4] have computed Lennard–Jones virial coefficients up to B_8. The Lennard–Jones seventh-order virial equation of state (LJ-VEOS7) yields a critical temperature in perfect agreement with the currently accepted value, 1.313(1) [5], and LJ-VEOS5 yields a critical temperature of 1.291, differing by only 1.7% from the currently accepted value. Thus, we expect that VEOS5 for an LJTS model would yield a reasonable estimate of the critical temperature and afford a means to examine the known effects of uncompensated truncation and shift upon it.

Here, we present virial coefficients of up to fifth order for several LJTS potentials. We employ these newly computed coefficients to estimate the critical temperature through the virial equation of state and the perturbed virial expansion (pVE) proposed by Nezbeda and Smith[6]. As seen in Eq. (*6*), the perturbations take the form of *n*-th order virial contributions, such that pVE1 considers the difference of reference and target second virial coefficients, pVE2 the difference of the second and third virial coefficients, etc.

$$\frac{P}{\rho kT} = \left(\frac{P}{\rho kT}\right)^{\mathrm{HS}} + \sum_{n=2}^{\infty} \left(B_n(T) - B_n^{\mathrm{HS}}\right) \rho^{n-1} \tag{6}$$

We employ the hard-sphere equation of state of Boublik and Nezbeda[7] as the reference with a hard-sphere diameter equal to the Lennard–Jones σ. Using a temperature-dependent hard-sphere diameter, Nezbeda and Smith[6] found LJ-pVE1 and LJ-pVE2 to yield good estimates of the critical temperature, kT_c/ε, of 1.27 and 1.28, respectively.

EXPERIMENTAL

In this work, we consider LJTS models with truncation distances of 2.5, 3.0, 4.0, 5.0, 6.0, 8.0, and 10.0σ. We compute B_2 to B_5 for each at reduced temperatures, kT/ε, spanning 0.7 to 2.0. For spherically symmetric potentials, B_2 and B_3 are trivial computations. Here, we have computed B_2 values using simple quadrature and B_3 values with fast Fourier transforms. As higher-order B_n are less amenable to quadrature (the number of integration variables increases by three with each increase in order), we compute B_4 and B_5 using Mayer-sampling Monte Carlo (MSMC).

We review the MSMC method only briefly, as a detailed description can be found elsewhere[8]. MSMC uses the same basic concept as free-energy perturbation methods: configuration integrals (e.g., virial coefficients) can be formulated as ratios of ensemble averages by introducing sampling weights. The sampling weight is selected to be the absolute value of the integrand because configurations having a larger integrand are more important to the calculation. The method was named Mayer sampling because, for pairwise additive potentials, the integrands of the virial coefficients are composed of pair Mayer functions, $f = e^{-u/kT} - 1$.

The original formulation of MSMC[9] employed direct sampling with a reference system of hard spheres. Hard-sphere virial coefficients can be determined readily by other methods, such as Ree–Hoover Monte Carlo sampling[10]. However, the Mayer functions of hard spheres and most soft potentials at low temperatures are quite different. As the Mayer function of Lennard–Jones is sharply peaked about the equilibrium separation distance at low temperatures, highly-overlapped configurations important to hard spheres are typically not sampled sufficiently. Overlap sampling avoids this difficulty[8] and has been used in subsequent works where hard spheres are employed as the reference system[11].

The important regions of configuration space for Lennard–Jones and truncated-and-shifted Lennard–Jones are similar even at low temperatures, making direct sampling feasible. In this case, the LJ coefficient is used as the reference quantity and the absolute value of its integrand as the sampling weight. The MSMC method is conducted in an infinite volume having no boundary, so sampling based on an untruncated potential introduces no complication. Moreover, it permits consideration of multiple LJTS potentials during a simulation: at each accepted configuration, the potential can be perturbed to as many LJTS potentials as desired. This constitutes a significant advantage over overlap sampling, in which a separate calculation is required for each truncation distance.

We have found that there is little difference in cpu time per step in calculations employing overlap sampling and direct sampling. Direct sampling within this context also provides the benefit of significantly lower standard errors when covariance is considered as the LJ and LJTS potentials yield highly correlated values at each configuration. This benefit increases with the truncation distance, as the LJ and LJTS potentials become more similar.

We have applied this direct-sampling approach to compute the B_4 and B_5 values presented in this work. The B_n^{LJ} values used as reference quantities were computed[5] by the overlap-sampling formulation of MSMC, referencing hard spheres. We have also applied the direct-sampling method to B_2 and B_3 to examine sampling efficiency relative to B_4 and B_5. We employed one hundred runs of 10^8 Monte Carlo steps for B_2 and B_3, and one hundred runs of 10^9 Monte Carlo steps for B_4 and B_5. At temperatures between 1.0 and 1.4, an additional four hundred runs were used for B_5 calculations.

RESULTS AND DISCUSSION

Virial Coefficients

In Tables I–IV, we present values of second, third, fourth, and fifth virial coefficients, respectively, and in Fig. 1, we plot the results. The lines are values interpolated using the method of Schultz and Kofke[12].

Across the temperature range and orders considered, there are significant differences between the LJ values and those of LJTS2.5 and LJTS3.0. The behavior of B_5 for these shorter truncation distances is particularly extreme. As the truncation distance increases, the LJTS values converge to those of LJ, but the rate of convergence is slower for the higher-order coefficients. This is understandable, in that the larger the number of molecules (the more pairs there are), the more the differences in the description of the pair interaction should manifest themselves. In Fig. 1, one can see that in increasing the order from third to fourth to fifth, the differences between LJTS4.0, LJTS5.0, LJTS6.0, and LJ become more noticeable, especially at

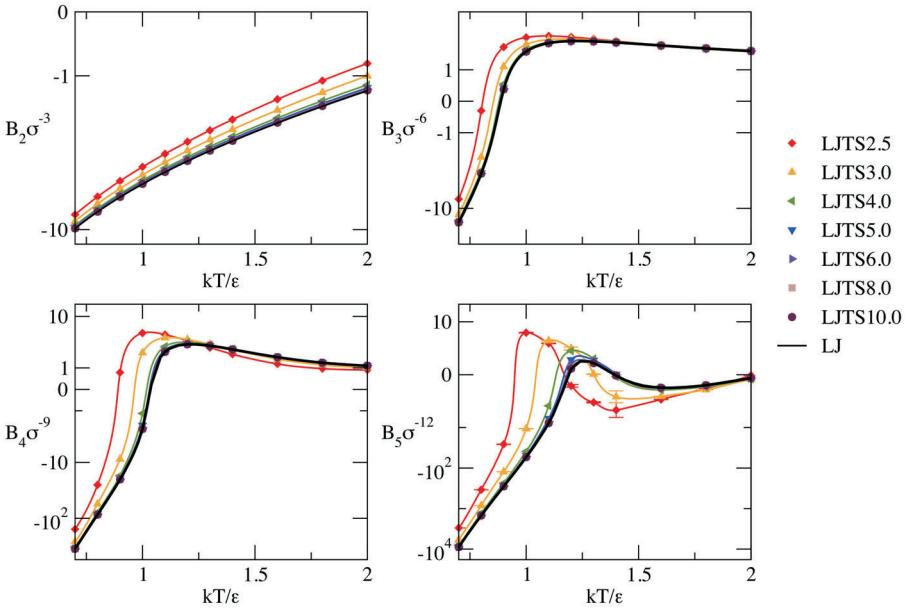

FIG. 1
LJTS virial coefficients of different truncation, plotted versus reduced temperature on an inverse hyperbolic-sine scale. Error bars are shown only if larger than the markers. The lines are values interpolated using the method of Schultz and Kofke[12]

TABLE I
Second virial coefficients for LJ and LJTS potentials computed by quadrature and rounded to the fifth decimal place

kT/ε	$B_2\sigma^{-3}$							
	LJTS2.5	LJTS3.0	LJTS4.0	LJTS5.0	LJTS6.0	LJTS8.0	LJTS10.0	LJ
0.7	–8.13320	–8.90666	–9.47734	–9.66964	–9.75267	–9.81772	–9.84069	–9.86468
0.8	–6.34432	–6.99610	–7.48447	–7.65093	–7.72315	–7.77989	–7.79996	–7.82094
0.9	–5.09324	–5.65703	–6.08431	–6.23115	–6.29507	–6.34539	–6.36322	–6.38186
1.0	–4.17187	–4.66896	–5.04897	–5.18037	–5.23772	–5.28294	–5.29897	–5.31575
1.1	–3.46654	–3.91126	–4.25355	–4.37248	–4.42449	–4.46554	–4.48011	–4.49536
1.2	–2.91014	–3.31259	–3.62406	–3.73270	–3.78029	–3.81788	–3.83123	–3.84520
1.3	–2.46059	–2.82821	–3.11400	–3.21400	–3.25786	–3.29253	–3.30484	–3.31774
1.4	–2.09023	–2.42861	–2.69268	–2.78531	–2.82599	–2.85816	–2.86959	–2.88157
1.6	–1.51692	–1.80897	–2.03824	–2.11900	–2.15452	–2.18264	–2.19264	–2.20312
1.8	–1.09484	–1.35181	–1.55443	–1.62602	–1.65754	–1.68252	–1.69141	–1.70072
2.0	–0.77201	–1.00147	–1.18302	–1.24732	–1.27566	–1.29812	–1.30612	–1.31450

TABLE II
Third virial coefficients for LJ and LJTS potentials computed by fast Fourier transforms and quadrature and rounded to the fifth decimal place

kT/ε	$B_3\sigma^{-6}$							
	LJTS2.5	LJTS3.0	LJTS4.0	LJTS5.0	LJTS6.0	LJTS8.0	LJTS10.0	LJ
0.7	–7.71683	–11.94502	–14.24138	–14.65765	–14.75967	–14.80260	–14.80952	–14.81199
0.8	–0.27026	–2.28641	–3.43291	–3.64517	–3.69752	–3.71961	–3.72318	–3.72446
0.9	2.15968	1.12139	0.49862	0.38069	0.35142	0.33903	0.33702	0.33631
1.0	2.89700	2.33835	1.98062	1.91115	1.89378	1.88641	1.88522	1.88479
1.1	3.02347	2.71809	2.50508	2.46248	2.45174	2.44717	2.44643	2.44616
1.2	2.92963	2.76527	2.63589	2.60906	2.60223	2.59932	2.59884	2.59867
1.3	2.76557	2.68275	2.60380	2.58664	2.58223	2.58034	2.58003	2.57992
1.4	2.59029	2.55580	2.50828	2.49727	2.49440	2.49316	2.49295	2.49288
1.6	2.28075	2.29281	2.27840	2.27406	2.27287	2.27235	2.27226	2.27223
1.8	2.04744	2.07579	2.07560	2.07429	2.07388	2.07369	2.07366	2.07365
2.0	1.87846	1.91120	1.91715	1.91727	1.91724	1.91721	1.91720	1.91720

TABLE III

Fourth virial coefficients for LJTS potentials computed by direct sampling and the LJ values computed by overlap sampling[4] and employed as the reference quantities. Numbers in parentheses are the 67% confidence limits in the rightmost digits of the value

kT/ε	$B_4\sigma^{-9}$							
	LJTS2.5	LJTS3.0	LJTS4.0	LJTS5.0	LJTS6.0	LJTS8.0	LJTS10.0	LJ
0.7	–156.98(3)	–260.85(2)	–331.380(19)	–346.160(19)	–349.910(19)	–351.500(19)	–351.760(19)	–351.854(19)
0.8	–25.284(13)	–55.497(9)	–78.528(7)	–83.723(7)	–85.070(7)	–85.648(7)	–85.742(7)	–85.776(7)
0.9	0.749(10)	–8.782(6)	–17.274(3)	–19.369(3)	–19.926(3)	–20.167(3)	–20.206(3)	–20.221(3)
1.0	5.018(19)	2.141(12)	–1.161(4)	–2.0776(16)	–2.3281(15)	–2.4378(15)	–2.4558(15)	–2.4623(15)
1.1	4.691(6)	4.100(5)	2.8306(16)	2.4094(8)	2.2899(7)	2.2369(7)	2.2281(7)	2.2250(7)
1.2	3.6282(16)	3.8189(14)	3.3933(8)	3.1973(7)	3.1387(6)	3.1122(6)	3.1078(6)	3.1062(6)
1.3	2.6854(8)	3.1095(7)	3.0443(4)	2.9564(3)	2.9278(3)	2.9145(3)	2.9123(3)	2.9115(3)
1.4	2.0012(4)	2.4533(4)	2.5376(4)	2.5030(4)	2.4898(4)	2.4833(4)	2.4823(4)	2.4818(4)
1.6	1.2455(3)	1.5892(2)	1.7400(2)	1.7451(2)	1.7440(2)	1.7431(2)	1.7429(2)	1.7429(2)
1.8	0.95863(19)	1.18040(16)	1.30970(5)	1.32300(15)	1.32500(15)	1.32570(15)	1.32580(15)	1.32578(15)
2.0	0.88299(14)	1.01590(12)	1.11200(11)	1.12500(11)	1.12750(11)	1.12840(11)	1.12850(11)	1.12860(11)

TABLE IV

Fifth virial coefficients for LJTS potentials computed by direct sampling and the LJ values computed by overlap sampling[4] and employed as the reference quantities. Numbers in parentheses are the 67% confidence limits in the rightmost digits of the value; 500 runs of 10^9 steps were employed for kT/ε = 1.0, 1.1, 1.2, 1.3, and 1.4, while 100 runs of 10^9 steps were employed at other temperatures

kT/ε	$B_5\sigma^{-12}$							
	LJTS2.5	LJTS3.0	LJTS4.0	LJTS5.0	LJTS6.0	LJTS8.0	LJTS10.0	LJ
0.7	–2998(3)	–5866(2)	–8129.3(1.8)	–8650.1(1.8)	–8787.8(1.8)	–8847.4(1.8)	–8857.0(1.8)	–8860.5(1.8)
0.8	–343.4(8)	–846.7(7)	–1310.3(5)	–1429.6(5)	–1462.6(5)	–1477.1(5)	–1479.5(5)	–1480.4(5)
0.9	–26.0(4)	–123.7(3)	–235.74(15)	–268.75(14)	–278.40(14)	–282.76(14)	–283.48(14)	–283.74(14)
1.0	5.38(10)	–10.70(9)	–39.02(6)	–49.12(6)	–52.31(6)	–53.78(6)	–54.03(6)	–54.12(6)
1.1	2.86(7)	3.37(8)	–2.84(4)	–5.99(2)	–7.10(2)	–7.64(3)	–7.74(3)	–7.77(3)
1.2	–0.68(9)	2.09(20)	1.79(16)	0.95(7)	0.58(4)	0.384(19)	0.350(17)	0.338(16)
1.3	–2.30(9)	0.027(17)	1.035(16)	0.904(12)	0.785(9)	0.715(8)	0.702(8)	0.698(8)
1.4	–3.7(13)	–1.6(6)	–0.12(3)	0.02(2)	–0.013(12)	–0.042(6)	–0.048(6)	–0.050(7)
1.6	–1.92(3)	–1.568(18)	–0.976(5)	–0.834(3)	–0.812(3)	–0.807(3)	–0.806(3)	–0.806(3)
1.8	–0.858(6)	–0.965(6)	–0.748(3)	–0.6590(18)	–0.6392(17)	–0.6322(17)	–0.6312(17)	–0.631(17)
2.0	–0.038(3)	–0.281(4)	–0.254(2)	–0.2103(13)	–0.1985(11)	–0.1940(11)	–0.1933(11)	–0.1931(11)

lower temperatures. Convergence to the LJ values with increasing truncation distance is generally slower for lower temperatures, though this is harder to deduce from the plots as the scale exaggerates differences close to zero. As the temperature increases, the short-range repulsive part of the potential becomes more important, diminishing the effect of truncation and shift on B_n.

Sampling Efficiency

One would expect that the longer the truncation distance is (the more similar the LJTS and LJ potentials are), the more efficient the direct-sampling calculation would be. This is what we observe for second through fifth virial coefficients, as can be seen in Fig. 2. In each subplot, the magnitude of the contribution to the standard error of a coefficient resulting from the ratio computed by MSMC is shown, divided by the value of the coefficients; in these subplots, we neglect the uncertainties in the reference values.

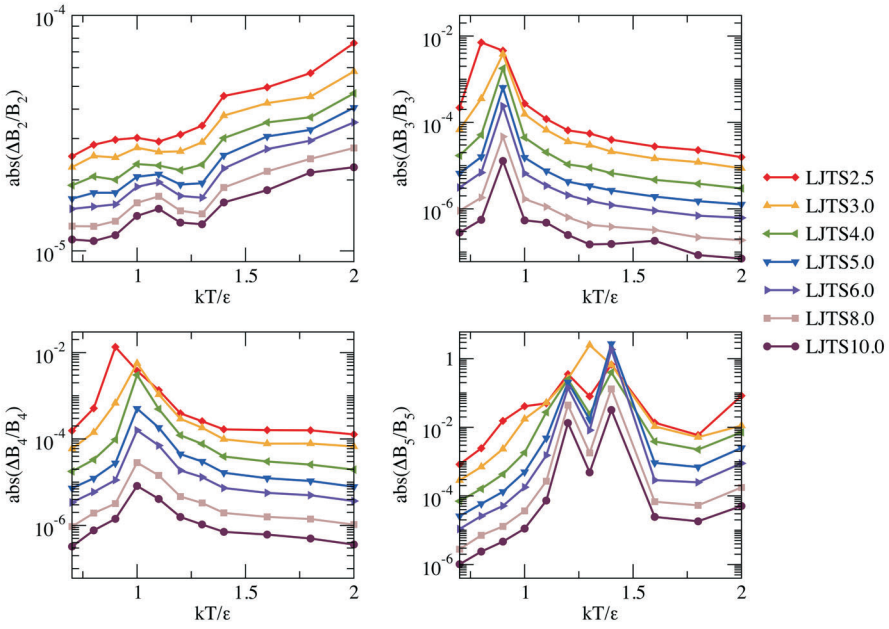

FIG. 2
Standard errors in the virial coefficients, neglecting any uncertainty in the reference values, normalized by the magnitude of the virial coefficient. The standard errors for B_5 do not include the additional four hundred runs at reduced temperatures between 1.0 and 1.4

As the truncation distance increases, these contributions to the standard error drop by orders of magnitude for all but B_2. It appears that increasing the truncation distance from 2.5 to 5.0σ, for example, has a larger impact on sampling efficiency for B_3, B_4, and B_5 than it does for B_2, further demonstrating that B_2 is less sensitive to truncation and shift. For B_4 and B_5, the standard errors resulting from the ratio computed by direct sampling drop well below the standard errors of the reference value: for these coefficients, the precisions we report in the tables and Fig. 1 are limited by that of the reference value.

Vapor-Branch Spinodals and Critical Points

We employ the computed virial coefficients within the virial equation of state and the perturbed virial expansion. The resulting spinodals are determined by locating zeros of the first derivative of the pressure with respect to density, and the critical points by locating the density at which the second derivative is also zero. In Fig. 3, we have plotted spinodals of LJ-VEOS5 and each LJTS-VEOS5 up to the critical point. Literature values for the criti-

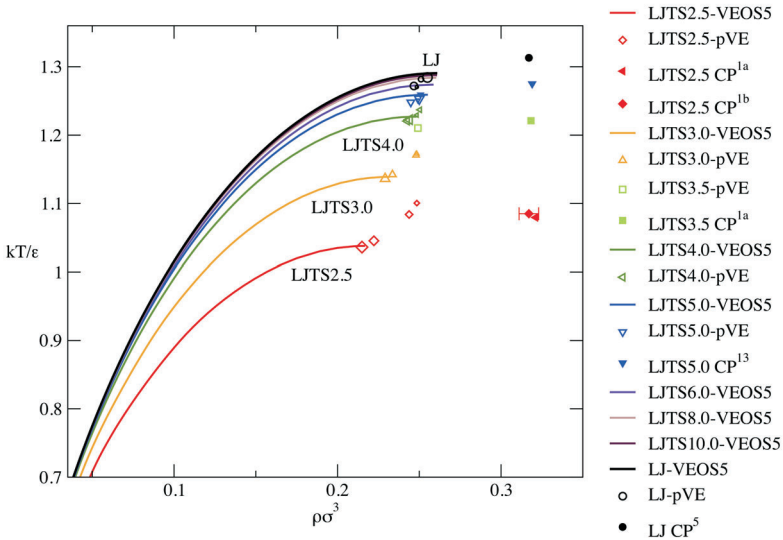

FIG. 3
VEOS5 vapor-branch spinodals plotted up to the resulting critical point (lines), critical points of perturbed virial expansions: pVE1 (smallest open symbols) to pVE4 (largest open symbols), and critical points computed either by Gibbs-ensemble Monte Carlo and scaling arguments (LJTS2.51, LJTS3.51a, LJ5) or temperature-quench molecular dynamics (LJTS5.013) (solid symbols)

cal points of LJ [5], LJTS2.5 [1], LJTS3.5 [1a], and LJTS5.0 [13] are included on the plot. In addition, we present critical points estimated using the first-, second-, third-, and fourth-order perturbed virial expansions. Nezbeda and Smith[6] report critical points for LJ-pVE1 ($kT_c/\varepsilon = 1.27$ and $\rho_c\sigma^3 = 0.249$) and LJ-pVE2 ($kT_c/\varepsilon = 1.28$ and $\rho_c\sigma^3 = 0.252$) that agree well with our values for LJ-pVE1 ($kT_c/\varepsilon = 1.2704$ and $\rho_c\sigma^3 = 0.24848$) and LJ-pVE2 ($kT_c/\varepsilon = 1.2817$ and $\rho_c\sigma^3 = 0.2511$) computed with a constant hard-sphere diameter of σ.

We observe that as the truncation distance decreases, the VEOS5 spinodal temperatures at a given density decrease, while the spinodal densities at a given temperature increase. This is in accordance with our expectations that, for a more repulsive potential, vapor should be metastable or stable over a wider range of conditions. As observed for the virial coefficients, the LJTS spinodals converge to that of LJ-VEOS5 as the truncation distance increases. However, apparent convergence to the LJ-VEOS5 spinodal across the range of conditions is not observed until a truncation distance of about 8.0σ. This is sensible, in that the spinodals reflect not only the temperature dependence of the virial coefficients but also the density dependence of each order's contribution, which is magnified on differentiation. The higher the density, the more the differences in the virial coefficients at a particular temperature should manifest themselves.

The spinodal of LJTS5.0-VEOS5 achieves good agreement with that of LJ-VEOS5 up to about half of the critical density, a region in which the fourth and fifth virial coefficients are likely unimportant. The VEOS5 critical temperature of LJTS5.0 differs from that of LJ by an amount almost five times smaller than the LJTS3.0 result does and more than eight times smaller than the LJTS2.5 result does, as shown in Table V. We observe the same for the pVE1 estimates of the critical temperature, shown in Table VI.

To estimate the uncertainty in VEOS5 critical properties resulting from that in the measured coefficients, we use the following scheme: for each order of virial coefficient, a Gaussian distribution for the virial coefficient is created with a standard deviation of the coefficient's standard error (in the case of B_4 and B_5) or its convergence error (in the case of B_2 and B_3). The distribution of each coefficient is sampled to generate a possible VEOS5, and the critical properties of this VEOS5 are computed. Performing the operation one hundred times for each potential model, we have noted that there is a bias in the distribution of critical temperatures and densities such that the average of the distribution is often smaller than the value computed with the average virial coefficients, which we consider to be our best estimate. This bias becomes worse as the truncation distance decreases. For that reason, the standard deviations we compute are relative to the best es-

timate and not the average of the distribution. These standard deviations are the uncertainties we report in Table V.

We must also consider the uncertainty associated with interpolation between the temperatures where the coefficients are evaluated. Values for B_n^{LJ} have been computed previously at a density of temperatures about five times that considered here, and the critical property values presented in Table V are computed from these values. Interpolating between only the temperatures employed in this work yields critical properties (kT_c/ε = 1.2909(3) and $\rho_c\sigma^3$ = 0.26120(18)) with sampling-scheme uncertainty estimates that are about the same as the differences from the critical properties computed with less interpolation. Thus, we conclude that interpolation between increments of kT/ε = 0.1 is largely sufficient for the unmodified potential. However, the fifth virial coefficient for the LJTS2.5 and LJTS3.0 models varies more widely in between 0.9 and 1.2, such that interpolating between increments of kT/ε = 0.1 might not be sufficient. Removing half of the temperatures below kT/ε = 1.6, either odd or even, we observe that a very conservative estimate of the uncertainty would be as much as an order of magnitude larger than the uncertainties we report in Table V.

TABLE V
VEOS5 critical points: temperatures, densities, and their per-cent differences relative to those of LJ-VEOS5 and, where possible, respective true values for each potential. Numbers in parentheses indicate the confidence limits of the last digit(s) of the tabulated value

Model	VEOS5		% difference from LJ-VEOS5 result		% difference from true value	
	kT_c/ε	$\rho_c\sigma^3$	kT_c/ε	$\rho_c\sigma^3$	kT_c/ε	$\rho_c\sigma^3$
LJTS2.5	1.038(2)	0.2168(16)	–19.58	–3.9[1a]	–16.92	–32.5[1a]
LJTS3.0	1.1389(11)	0.2319(8)	–11.75		–11.14	
LJTS4.0	1.2270(12)	0.2484(9)	–4.93		–4.84	
LJTS5.0	1.2591(6)	0.2552(4)	–2.44	–1.3[13]	–2.21	–20.0[13]
LJTS6.0	1.2738(3)	0.2587(3)	–1.30		–0.87	
LJTS8.0	1.2840(3)	0.2604(3)	–0.51		–0.22	
LJTS10.0	1.2875(4)	0.2609(2)	–0.24		–0.04	
LJ	1.29058(9)	0.26098(7)	0.00	–1.7[5]	0.00	–17.7[5]

Truncation and shift is known to suppress the critical temperature but not alter the critical density. The fourth columns of Tables V and VI compare the VEOS5 and pVE1 critical temperatures and densities to true values for the respective potentials available in the literature. Agreement with the true critical temperatures of LJTS2.5, LJTS5.0, and LJ is within a few percent for both approximations. Remarkably, the pVE1 estimate of the critical point of LJTS2.5 is superior to the estimate of VEOS5. The pVE1 values correctly capture the temperature trend as well as the insensitivity of the critical density to the truncation distance (although the value of the critical density is inaccurate). One can show that the critical density of pVE1 is indeed independent of truncation radius, and the critical temperature can be obtained by solving for the temperature at which B_2 for the truncated potential equals B_2 for the untruncated potential at its critical temperature (i.e., $B_2^{\mathrm{LJTS}}(T_c^{\mathrm{LJTS}}) = B_2^{\mathrm{LJ}}(T_c^{\mathrm{LJ}})$).

VEOS5 captures the suppression of critical temperature with decreasing truncation distance, but the predicted critical densities diminish systematically with the truncation distance and at a rate greater than could be explained by uncertainties due to standard error in the coefficients or the interpolation scheme. Moreover, higher-order pVE estimates generally do not improve upon the accuracy of pVE1: these appear to converge to the values obtained by VEOSn rather than the true critical points. Addition of higher terms to the expansion diminishes the significance of the reference hard-sphere system (as it is systematically removed with each added term), and makes the perturbation model increasingly like the virial equation it-

TABLE VI
pVE1 critical points: temperatures, densities, and their percent differences relative to those of LJ-pVE1 and, where possible, respective true values for each potential

Model	pVE1		% difference from LJ-pVE1 result	% difference from true value	
	kT_c/ε	$\rho_c\sigma^3$	kT_c/ε	kT_c/ε	$\rho_c\sigma^3$
LJTS2.5	1.1005	0.24848	–13.37	1.95[1a]	–22.62[1a]
LJTS3.0	1.1726	0.24848	–7.70		
LJTS5.0	1.2494	0.24848	–1.66	–2.01[13]	–22.11[13]
LJ	1.2704	0.24848	0	–3.25[5]	–21.62[5]

self. Nevertheless, the reference system can retain its relevance at densities higher than considered here.

The accuracy of a critical point obtained at a given order by either treatment appears to diminish as the truncation distance decreases. In Fig. 4, we plot the vapor-branch spinodals of VEOS3, VEOS4, and VEOS5 for LJTS2.5, LJTS3.0, and LJ as well as the corresponding critical points predicted by the analogous perturbed virial expansions (pVE2, pVE3, and pVE4, respectively). Increasing the truncation distance from 2.5 to 3.0σ to ∞, the significance of the fifth-order VEOS contribution diminishes, as demonstrated by the respective percent differences in the critical temperature (–6.7, –6.2, –2.4%) and the critical density (1.8, 1.7, 0.6%). This larger fifth-order contribution for LJTS2.5 and LJTS3.0 is likely the result of their lower spinodal temperatures, where the virial coefficients are generally larger and more negative.

Though we do not observe convergence, it is possible that the accuracy of the critical points to which both treatments converge diminishes as the truncation distance decreases. The pVE critical points appear to converge more quickly than those of VEOSn: for each potential, the critical point of pVE2 is much closer to that of pVE4 than the critical point of VEOS3 is to

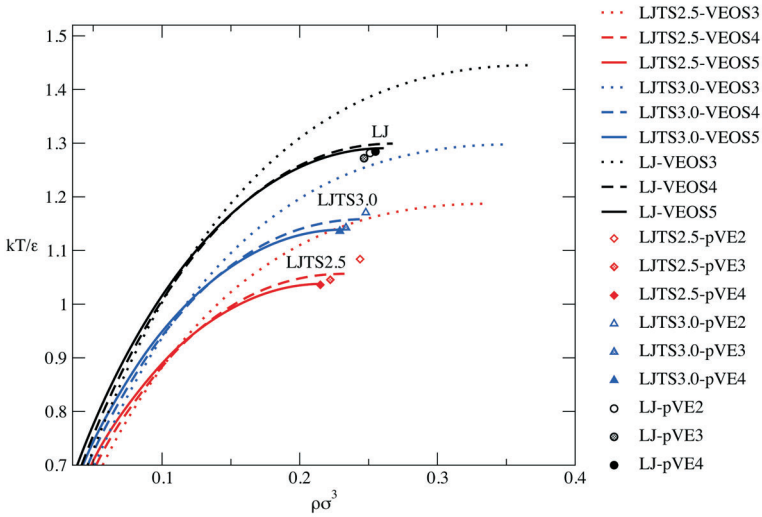

FIG. 4

Vapor-branch spinodals from VEOS3 (dotted lines), VEOS4 (dashed lines), and VEOS5 (solid lines) for LJTS2.5 (red), LJTS3.0 (blue), and LJ (black), plotted up to the resulting critical point. Also shown are critical points computed from pVE2 (open symbols), pVE3 (cross-hatch symbols), and pVE4 (solid symbols)

that VEOS5. The pVE perturbs from a reference of hard spheres, while the VEOS perturbs from the ideal gas; thus we may consider that the pVE has a better starting point for the perturbation.

CONCLUSIONS

Truncation and shift result in a more repulsive pair potential, and thus virial coefficients that are generally more positive, especially at low temperatures. The higher the order of a virial coefficient (the more pair interactions it describes), the more sensitive it is to modification of the pair potential. As higher-order interactions become more relevant, either upon increasing the order of a virial coefficient or increasing the density at which a bulk property is evaluated, one should expect differences in values computed from LJTS and LJ potentials to increase. As much is observed here for the spinodals computed from VEOS5: as the density increases, LJTS-VEOS5 spinodals of increasing truncation distance peel away from the VEOS5 spinodal of the unmodified potential. The VEOS5 spinodals for the popular truncation distances of 2.5 and 3.0σ begin to differ markedly from that of LJ well below a third of the critical density, and ultimately result in VEOS5 critical temperatures that are 20 and 12% lower, respectively.

The critical points of the virial equation of state and the perturbed virial expansion appear to be converging to similar values that are not coincident with the true critical point, or at least not with the true critical density. The perturbed virial expansion considered here appears to be converging more rapidly, most likely because it is perturbing from a more accurate reference (hard spheres) than the virial equation of state is. The ability of both treatments to predict the critical point appears to diminish as the truncation distance decreases, though they capture the correct trend of shorter truncations suppressing the critical temperature. The perturbed virial expansion (except at first order) and the virial equation of state do not demonstrate the insensitivity of the critical density to truncation distance.

Funding for this research was provided by grant CHE-0626305 from the U.S. National Science Foundation, and by the University at Buffalo School of Engineering and Applied Sciences. Computational support was provided by the University at Buffalo Center for Computational Research.

REFERENCES

1. a) Shi W., Johnson J. K.: *Fluid Phase Equilib.* **2001**, *187–188*, 171; b) Smit B.: *J. Chem. Phys.* **1992**, *96*, 8639.
2. Kolafa J., Nezbeda I.: *Fluid Phase Equilib.* **1994**, *100*, 1.

3. Frenkel D., Smit B.: *Understanding Molecular Simulation: From Algorithms to Applications*. Academic Press, San Diego 1996.
4. Schultz A. J., Kofke D. A.: *Mol. Phys.* **2009**, *107*, 2309.
5. Perez-Pellitero J., Ungerer P., Orkoulas G., Mackie A. D.: *J. Chem. Phys.* **2006**, *125*, 054515.
6. Nezbeda I., Smith W. R.: *Fluid Phase Equilib.* **2004**, *216*, 183.
7. Boublik T., Nezbeda, I.: *Collect. Czech. Chem. Commun.* **1986**, *51*, 2301.
8. Benjamin K. M., Singh J. K., Schultz A. J., Kofke D. A.: *J. Phys. Chem. B* **2007**, *111*, 11463.
9. Singh J. K., Kofke D. A.: *Phys. Rev. Lett.* **2004**, *92*, 220601.
10. Ree F. H., Hoover W. G.: *J. Chem. Phys.* **1964**, *40*, 939.
11. a) Benjamin K. M., Schultz A. J., Kofke D. A.: *J. Phys. Chem. B* **2009**, *113*, 7810; b) Benjamin K. M., Schultz A. J., Kofke D. A.: *J. Phys. Chem. C* **2007**, *111*, 16021.
12. Schultz A. J., Kofke D. A.: *Mol. Phys.* **2009**, *107*, 1431.
13. Martinez-Veracoechea F., Muller E. A.: *Mol. Simul.* **2005**, *31*, 33.